THE JOURNAL OF PHYSICAL CHEMISTRY B

Article

pubs.acs.org/JPCB

Determination of Structural Characteristics of All-Organic Radical Liquid Crystals Based on Analysis of the Dipole−Dipole Broadened EPR Spectra

A. Kh. Vorobiev,*[,†] N. A. Chumakova,[†] D. A. Pomogailo,[†] Y. Uchida,[‡] K. Suzuki,[‡] Y. Noda,[‡] and R. Tamura[‡]

[†]Department of Chemistry, M.V. Lomonosov Moscow State University, Moscow 119992, Russian Federation

[‡]Graduate School of Human and Environmental Studies, Kyoto University, Kyoto 606-8501, Japan

ABSTRACT: The angular dependences of g-value and line width of EPR spectra of paramagnetic all-organic liquid crystalline (LC) materials were measured for the quantitative characterization of the nematic, cholesteric, and smectic C phases. The detailed molecular alignment in mesophases was determined by means of numerical spectra simulation focusing on spin exchange and dipole−dipole magnetic interactions of neighboring molecules. The obtained structural data indicate that the spin polarization mechanism between neighboring molecules rather than the direct through-space interactions between paramagnetic centers is responsible for the specific magnetic properties of the studied LC materials.

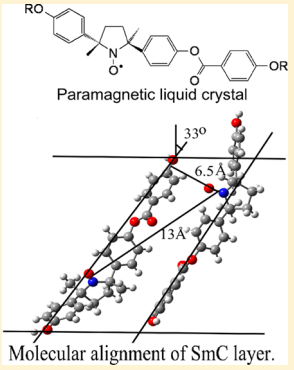

1. INTRODUCTION

Liquid crystals (LCs) are widely used in display technologies and are being considered for many potential applications, such as optical data storage materials, active optical media, biomedical tools, and so on.[1−4] LCs are sensitive to external stimuli, such as temperature, pressure, and electric and magnetic fields, or additives, such as chiral dopants, and thereby the molecular orientation and LC superstructure can be easily altered.[5−8] In this context, magnetic LCs have been anticipated to become novel advanced soft materials that can combine the optical and electrical properties of conventional LCs with the magnetic and electronic properties of paramagnetic compounds, exhibiting unique magnetic interactions and unconventional magneto-electric[9−11] or magnetooptical[12−14] properties.

Meanwhile, the use of a thermally and air-stable nitroxide radical group as the spin source in the mesogen core of magnetic LCs is of great advantage for directly obtaining microscopic information on the molecular orientation, relative molecular position, and intermolecular magnetic interactions in the LC phases by electron paramagnetic resonance (EPR) spectroscopy, whereas X-ray diffraction, neutron scattering,[15,16] and optical techniques[17,18] are useful for the general characterization of the symmetry and type of LC phase. The spin exchange and dipole−dipole interactions of paramagnetic centers, which reflect the molecular structure of the material, manifest themselves in the shape of the EPR spectrum.[19] Thus, many reports have been devoted to the theoretical and experimental studies of dipole−dipole and exchange broadening of EPR spectra,[20−29] but in most cases the diluted isotropic solutions of a paramagnetic substance in a diamagnetic host medium have been considered. However, it is noteworthy that the known theories can essentially provide a good background to the quantitative description of EPR spectra of nondiluted paramagnetic LC samples.

With this situation in mind, we synthesized prototypic all-organic radical LC materials containing a nitroxide moiety in the rigid core part (Figure 1) and discovered the occurrence of the

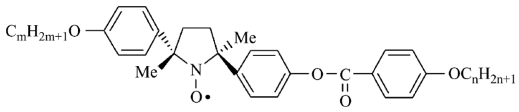

1: m = 7, n = 8 **2**: m = n = 13 **3**: m=n=4

Figure 1. Paramagnetic LC compounds used in the present study.

positive "magneto-LC effects" ($\bar{J} > 0$), a sort of spin glasslike inhomogeneous ferromagnetic interaction induced by weak magnetic fields, in the LC phases.[30−37] The understanding of the origin of the magneto-LC effects is essential for the design of LC molecules showing larger magnetic interactions. The aim of the present work is to extract the detailed structural information of magnetic LC phases from the shape and angular dependence of EPR spectra of paramagnetic LC materials and to study the origin of the positive magneto-LC effects.

We already reported the high sensitivity of the EPR technique in the determination of orientation molecular distribution when

Received: November 5, 2013
Revised: January 29, 2014
Published: January 30, 2014

substances shown in Figure 1 were used as paramagnetic probes in a diamagnetic host LC medium.[38,39] Although the specific angular dependence of the observed g-value of the EPR signal was reported as well,[40,41] the angular dependence of EPR spectrum broadening that demonstrates intermolecular magnetic interactions has not been analyzed yet.

2. EXPERIMENTAL DETAILS

We prepared (±)-**1**, (*S*,*S*)-**1**, (±)-**2**, (*S*,*S*)-**2**, and (*S*,*S*)-**3** as reported previously.[30,31] The phase sequences of samples **1** and **2** are as follows: crystal-(63.3 °C)-N-(103.1 °C)-isotropic for (±)-**1**, crystal-(79.3 °C)-N*-(103.5 °C)-isotropic for (*S*,*S*)-**1**, crystal-(71.9 °C)-SmC-(86.1 °C)-N-(90.3 °C)-isotropic for (±)-**2**, crystal-(67.2 °C)-SmC*-(86.0 °C)-N*-(90.8 °C)-isotropic for (*S*,*S*)-**2**, where N, N*, SmC, and SmC* denote the nematic, cholesteric (chiral nematic), smectic, and chiral smectic phases, respectively.

We used a commercially available thin-sandwich LC cell (EHC Co., Japan; 4 μm thickness) that consists of two indium tin oxide coated glass plates covered with rubbed polyimide films. The cell gap was maintained by inserting 4 μm thick spacers between the two plates. Substance was filled into the cell gap in the isotropic phase by capillary action under vacuum, and then the cell was cooled to room temperature. As shown in Figure 2a, the cell size

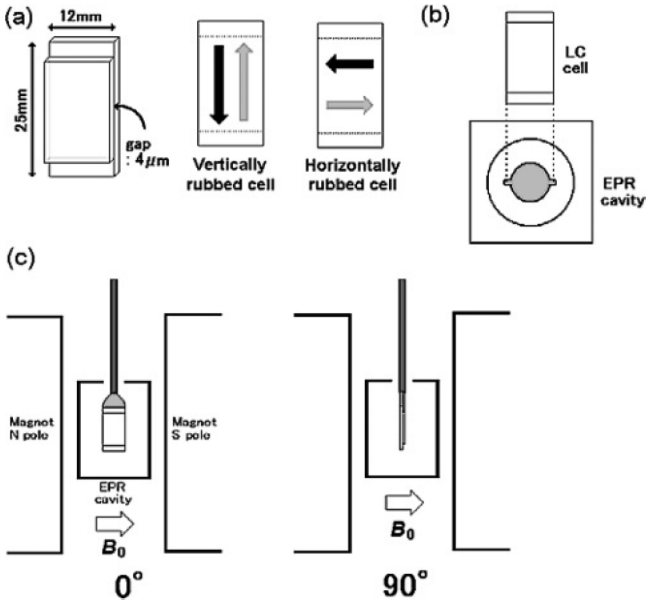

Figure 2. (a) (left) LC cell appearance and vertically and horizontally rubbed cells (middle and right, respectively). The black and gray arrows indicate the rubbing direction of the top and bottom planes, respectively. (b) Top view of the EPR cavity, which was designed for the insertion and rotation of the LC cell. (c) Definition of the rotation angles of the LC cell relative to the magnetic field of the spectrometer.

was 25 × 12 mm^2, and the rubbing directions on the top and the bottom planes were opposite (antiparallel configuration). To obtain the two-axis rotation data, we used two types of cells with different rubbing directions that were orthogonal to each other. As shown in Figure 2a, we defined one as vertically rubbed cell and the other as horizontally rubbed cell.

We used an EPR spectrometer (X-band, JEOL-FE1XG) with a cavity hole modified for LC cell insertion (Figure 2b). The modification of the insertion hole did not cause a critical loss of the Q-factor. We measured the EPR spectrum at each angle by rotating the rod to which the LC cell was attached. The angle was defined as 0° when the cell plane was parallel to the applied static magnetic field (Figure 2c). We constructed a temperature control system in which the sample was heated by the air flow. The system had two thermocouples: one is for monitoring the temperature near the heater, and the other is for monitoring the temperature near the LC cell. The temperature inhomogeneity in the cell area was estimated to be less than 1.5 °C. Spectra were recorded at the temperature of existence of mesophases.

3. EXPERIMENTAL RESULTS

Typical experimental spectra obtained are presented in Figure 3a. It is seen that the observed spectra are broadened singlet signals. Peak-to-peak line width is in the 1.6−1.9 mT range for smectic phases and in the 1.5−1.7 mT range for nematic phases. The values of line width directly measured using maximum and minimum points of the spectra were found to be insufficiently accurate for quantitative analysis. The errors are induced by noise of spectra recording. To obtain more precise quantitative characteristics of the spectra, the nonlinear least-squares fitting was used. The program described in ref 42 was applied for this procedure. The line shape was described by the Voigt profile, which is the convolution of Lorentzian and Gaussian functions. The g-value, Lorentzian width ΔH_L, and Gaussian width ΔH_G were varied parameters in the course of fitting.

The results of the fitting are illustrated in Figure 3a. The effective peak-to-peak width ΔH_{pp} of the signal was determined in accordance with the following equation:[43,44]

$$\left(\frac{\Delta H_G}{\Delta H_{pp}}\right)^2 + \frac{\Delta H_L}{\Delta H_{pp}} = 1 \quad (1)$$

The examples of obtained values of line widths for experimental spectra are presented in Table 1 (columns 2−4).

Spectra obtained experimentally were described within the precision of the recording procedure as it is seen in Figure 3a. The exceptions were the spectra of nematic phases recorded at 45° and 60°. These spectra were found to contain small admixture of dispersion spectrum, which has integral line shape. This admixture seems to be a result of the "rapid passage" effect.[45]

As a result of the fitting, the angular dependences of g-value and line width of signal were extracted from experimental spectra. The obtained data will be discussed below.

Singlet spectra are not typical for nitroxide radicals which ordinarily demonstrate hyperfine splitting on the nitrogen nucleus. The obvious causes of singlet signal in the studied LC materials are exchange interaction and rotation mobility that averages anisotropy of hyperfine interaction. To clarify the role of rotation movements, the following experiments were done. The spectrum of dilute disordered toluene solution of (±)-**2** at 77 K in glassy state was used to determine the anisotropic magnetic parameters. The obtained values were $g_x = 2.0091 \pm 0.0002$, $g_y = 2.0061 \pm 0.0002$, $g_z = 2.0021 \pm 0.0002$, $A_x = A_y = 0.39 \pm 0.05$ mT, and $A_z = 3.21 \pm 0.04$ mT. To study the molecular rotation mobility in an LC medium, the spectrum of diluted disordered solution of racemic compound (±)-**2** in the SmA phase of 8CB was recorded (Figure 3b). The simulation of this spectrum with the method[46,47] produced the following data: the tilt angles for main rotation molecular axis in g-tensor frame are $\alpha = 90°$ and $\beta = 39.6°$, and rotation diffusion coefficients are $D_x = D_y = (2.7 \pm 0.4) \times 10^6$ s^{-1} and $D_z = (3.0 \pm 0.3) \times 10^8$ s^{-1}. The obtained tilt angles are in accordance with the direction of elongated

dx.doi.org/10.1021/jp410891s | J. Phys. Chem. B 2014, 118, 1932−1942

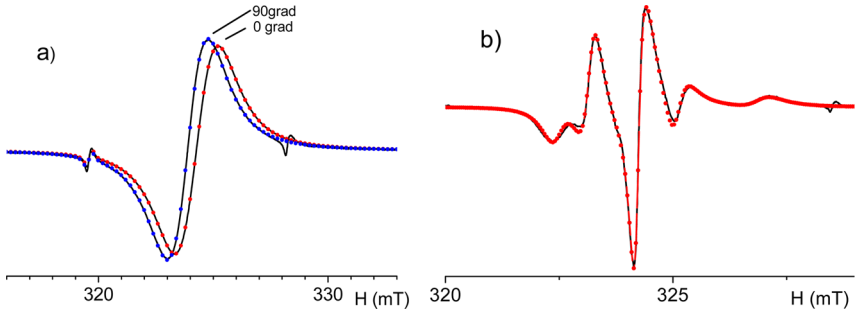

Figure 3. (a) Typical experimental EPR spectra and results of fitting using Voigt line shape. (b) EPR spectrum for diluted solution of (±)-**2** in the SmA phase of 8CB at 30 °C. Lines, experimental values; points, result of simulation.

Table 1. Lorentzian Width ΔH_L, Gaussian Width ΔH_G, and Peak-to-Peak Width ΔH_{pp} Obtained for Experimental Spectra (SmC) and Spectra Calculated Theoretically Using Eq 12 and Reverse Fourier Transform[a]

	experimental			calculated		
angle	ΔH_G	ΔH_L	ΔH_{pp}	ΔH_G	ΔH_L	ΔH_{pp}
0	9.16	14.45	18.89	8.92	14.52	18.76
30	7.84	15.55	18.81	8.83	14.53	18.70
60	7.07	15.68	18.40	8.26	14.57	18.30
90	7.41	14.64	17.74	7.08	14.87	17.70

[a]Parameters are listed in Table 3.

molecular axis in the magnetic molecular frame of nitroxide moiety and conform to the data obtained earlier.[38,39] The values of diffusion coefficients demonstrate that rotation around the long molecular axis is substantially faster than rotation around the perpendicular molecular axes.

4. QUALITATIVE CONSIDERATION OF EPR SPECTRUM LINE SHAPE

Figure 3b demonstrates the shape of EPR spectrum when dipole−dipole and exchange interactions are excluded. The fast rotation around the long molecular axis averages the magnetic parameters to the following values: $g^R_{xx} = g^R_{yy} = 2.0068$, $g^R_{zz} = 2.0037$, $A^R_{xx} = A^R_{yy} = 0.94$ mT, and $A^R_{zz} = 2.03$ mT (see Appendix A). The stochastic magnetic field from neighboring paramagnetic molecules can broaden the spectrum but cannot induce the disappearance of hyperfine splitting. Thus, absence of the splitting can be used for estimation of exchange frequency. It is known[19] that the hyperfine structure is collapsed when exchange frequency ω_{ex} is comparable to or more than the constant of hyperfine interaction ($\omega_{ex} \geq \gamma_e a$, where a is the hyperfine constant and γ_e is the electron gyromagnetic ratio). In the considered case this condition gives an estimate of exchange frequency $\omega_{ex} > 1.2 \times 10^8$ s^{-1}.

Let us estimate the collision frequency of paramagnetic fragments in the course of rotation movements. The molecular structure in the first coordination sphere of a molecule within the smectic layer can be considered as hexagonal close packing. The elementary rotational jump of a molecule in this structure is the turn around the long molecular axis with the angle $\lambda = \pi/3$. The simple model of random walk predicts the diffusion coefficient for rotation around this single axis to be equal to $D_r = \nu\lambda^2/2$, where ν is the jump frequency. The paramagnetic nitroxide group in the considered molecules is directed laterally relative to the long molecular axis. In the course of rotational jumps, the paramagnetic group comes into collision, which induces the change of spin state by exchange interaction. Therefore, the lifetime of a paramagnetic molecule in any spin state is determined by the frequency of rotational jumps. Using the experimentally obtained value of rotation diffusion coefficient $D_z = 3.0 \times 10^8$ s^{-1} and a factor of two for the probability of exchange after a jump, one can obtain the value for lifetime of spin state $\tau = 3.6 \times 10^{-9}$ s and predict the width of EPR line due to spin exchange ($\hbar/\gamma_e\tau$) ≈ 1.5 mT. Thus, the observed line width of EPR signal (1.6−1.9 mT) is determined mostly by the frequency of rotational collisions which induce the change of spin state by spin exchange with neighboring paramagnetic molecules. These rotations and exchange are characterized by the frequency that is sufficient to average the stochastic magnetic fields from neighboring particles, i.e., lead to zero dipole−dipole broadening of EPR spectra. There is one exception for this averaging process. It is the dipole−dipole interaction between neighboring molecules that are in exchange coupling. These molecules compose a combined multispin system in which dipole−dipole interaction of spins is not averaged but is a source of fine structure of EPR spectrum. Therefore dipole−dipole interaction of only a few molecules that are in exchange coupling should be taken into account in the course of the description of the shape of the EPR spectrum.

5. SUPERSTRUCTURE OF LIQUID CRYSTALLINE PHASES

To describe the angular dependences of g-value and line width obtained experimentally, the orientation order and mutual arrangement of molecules should be taken into account. For this purpose the structure of the liquid crystalline phase should be considered. The simplest structure is known to be in the nematic phase ((±)-**1** compound). The schematic presentation of this structure in the case of command surface oriented vertically is presented in Figure 4a.

Let Zs denote the sample axis oriented along the rubbing direction of the cell and Ys denote the sample axis oriented along the sample normal. Then, according to Figure 2c, the vertically aligned LC cell is rotated inside the ESR spectrometer cavity

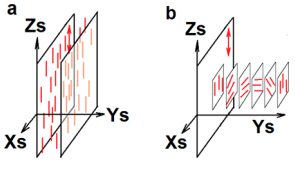

Figure 4. Schematic representation of molecular structures of nematic (a) and cholesteric (N*) (b) phases in the cell with command surfaces oriented vertically. Xs, Ys, and Zs are axes of the sample.

dx.doi.org/10.1021/jp410891s | J. Phys. Chem. B 2014, 118, 1932−1942

around its Zs axis, whereas the horizontally aligned LC cell is rotated around its Xs axis. The angular dependences of ESR spectra under these rotations will be further referred to as Z-dependence and X-dependence accordingly.

Preferential molecular orientation induced by rubbed command surfaces can be described by single-particle orientation distribution function $\rho_s(\beta,\gamma) = \partial N/\partial\beta\partial\gamma$, which describes number density of molecules oriented at Euler angles β and γ in the sample reference frame. The most general presentation of this function is expansion in a series of generalized spherical harmonics (elements of Wigner's D-matrix).[17,48] However, we will use here the simplest representation of orientation distribution function restricted by terms of the second rank:

$$\rho_s(\beta, \gamma) = \frac{1}{2} + \frac{5}{2}S_{20}P_2(\cos\beta) + \frac{5}{2\sqrt{6}}S_{22}P_2^2(\cos\beta)\cos 2\gamma \quad (2)$$

where S_{20} and S_{22} are orientation order parameters and $P_2(\cos\beta)$ and $P_2^2(\cos\beta)$ are Legendre polynomial and associated Legendre polynomial, respectively.

In the case of N* mesophase (compound (*S*,*S*)-**1**), the command surface induces orientation order only in the nearest layer of liquid crystal. The following layers are oriented with some angular shifts so that a helical orientation structure is formed in the medium (Figure 4b). The step of the helical structure is dictated by the twist power of the compound, but in the considered cells helical structure must also be consistent with the orientation imposed by the second command surface (not shown in Figure 4b for simplicity).

A more complicated structure is typical for smectic C phase (compound (±)-**2**). The structure of this mesophase must satisfy not only the orientation boundary condition induced by the command surface but also requirements of layer structure and tilt angle of molecules relative to the layer normal. The possible structures are presented in Figure 5.

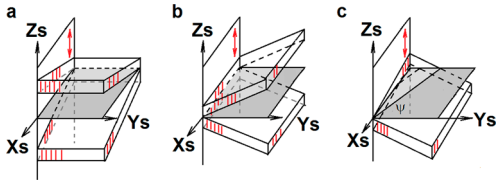

Figure 5. Schematic presentation of possible SmC structures in the cell. Limit case 1 (a) and limit case 2 (b) correspond to parallel and tilted orientation of C-director relative to the command surface. Only one of four possible layers in general case (c) is shown for clarity.

In Figure 5a and 5b, limit cases 1 and 2, which correspond to different orientations of layers relative to the command surface, are shown. Both limit cases permit the existence of two layers with different spatial orientations. In the general case, there are four possible layers with different orientations (only one of them is presented in Figure 5c). To describe possible spatial orientations of layers, let us consider the XsYs plane, which is orthogonal to the director of the command surfaces (gray planes in Figure 5). Then spatial orientations of layers can be described by angle ψ between the axis Ys and line of intersection of the layer and plane XsYs. Limit case 1 and limit case 2 are described by $\psi = 0$ and $\psi = \pi/2$, respectively.

Consideration of dipole−dipole interaction requires definition of not one-particle orientation distribution but mostly length and direction of vector connecting nitroxide groups of two neighboring molecules. To determine these parameters, let us consider the structure of the SmC layer in more detail. The molecules forming the layer are tilted relative to the layer normal. The direction of the tilt is defined by the C-director. Figure 6

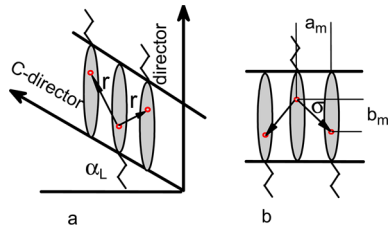

Figure 6. Mutual location of LC molecules in layer of SmC phase along C-director (a) and in perpendicular direction (b). Circles denote the positions of paramagnetic nitroxide groups.

demonstrates neighboring molecules in two orthogonal planes. The first plane (Figure 6a) contains the director and C-director of smectic layer. The second plane (Figure 6b) contains the director, but it is orthogonal to the first plane. It is known (see, for example, ref 49) that molecules in the monolayer smectics on the average have antiparallel orientation.

In order to describe the molecular structure of the smectic layer, we have chosen distances a_m and b_m and angle σ as parameters (see Figure 6b). These parameters are interdependent as $\tan\sigma = b_m/a_m$. The additional parameter α_L is the tilt angle of molecular axis relative to the smectic layer normal. Vectors **r** in Figure 6a connect the nitroxide groups of neighboring molecules. All defined parameters fluctuate in the real structure of LC. Thus, they are values averaged over orientational and positional molecular distributions.

Tilt α_L in SmC structure causes a dependence of vector **r** length on direction to neighboring molecules. To describe this dependence, the line of intersection of the layer and plane XsYs in Figure 5 can be used. Let φ be the angle between this line of intersection in Figure 5 and the projection of **r** on the plane XsYs. Then components of vector **r** in the sample reference frame (Xs, Ys, Zs) are the following (see Appendix C):

$$\{r_x, r_y, r_z\} = \{a_m\sin(\varphi - \psi), a_m\cos(\varphi - \psi), \pm (b_m + a_m\sin\varphi\, tg\alpha_L)\} \quad (3)$$

where ± reflects two locations of the layer relative to the plane XsYs in Figure 5.

Direction cosines for the vector **r** are the following:

$$\cos\mathbf{r} = \{\cos xr, \cos yr, \cos zr\} = \{\mathbf{r}_x/|\mathbf{r}|, \mathbf{r}_y/|\mathbf{r}|, \mathbf{r}_z/|\mathbf{r}|\} \quad (4)$$

where $|\mathbf{r}| = (r_x^2 + r_y^2 + r_z^2)^{1/2}$

Prediction of molecular structure of SmC* (compound (*S*,*S*)-**2**) in the considered cell is the most complicated problem. The requirement of molecular orientation induced by command surfaces of the cell, the requirement of the existence of smectic layers, and the requirement of helical orientation of C-director induced by optical activity of the compound cannot be satisfied simultaneously. It means that the real structure violates these requirements in some degree. As a result of the impossibility of predicting the real structure in these conditions, we cannot qualitatively describe angular dependences of line width obtained for this system.

dx.doi.org/10.1021/jp410891s | J. Phys. Chem. B 2014, 118, 1932−1942

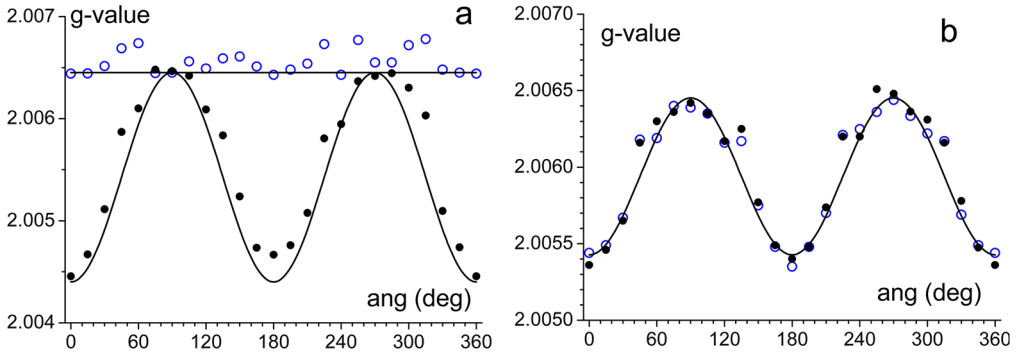

Figure 7. Angular dependences of g-value for N (a) and N* (b) phases obtained by description of experimental spectra. Solid points represent rotation around the Xs axis; open points represent rotation around the Zs axis; lines are results of calculations (see text).

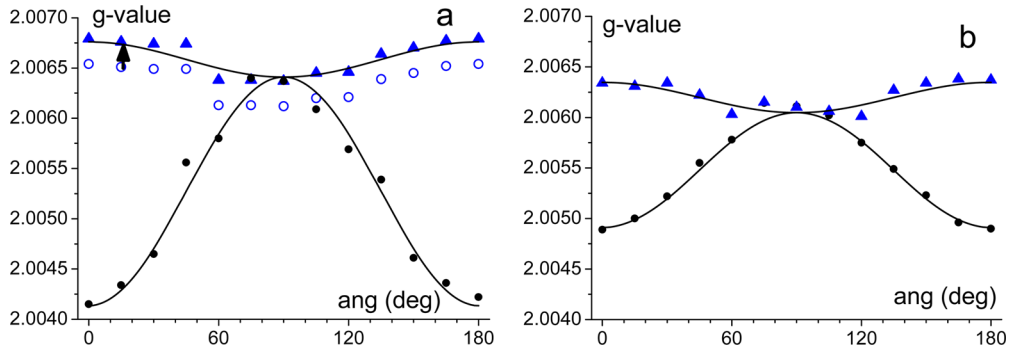

Figure 8. Angular dependences of g-value for SmC (a) and SmC* (b) phases obtained by description of experimental spectra. Solid points represent rotation around the Xs axis (X-dependence), and open points represent rotation around the Zs axis (Z-dependence). Triangles are Z-dependences shifted up 0.00025, and lines are results of calculations (see text).

6. DESCRIPTION OF G-VALUE ANGULAR DEPENDENCES

Angular dependences of g-value for N and N* phases obtained by fitting of experimental spectra are presented in Figure 7.

To calculate angular dependence of the g-value presented in Figure 7a, one should take into account that the anisotropy of the g-value is smaller than the width of the EPR spectrum observed. The signals from particles with different orientations overlap and form a single resonant line. In this condition the direct averaging of the g-value with orientation distribution is valid. Let $\mathbf{g}_{rf}^2$ be the effective $\mathbf{g}^2$-tensor presented in the reference frame of rotation axes (see Appendix A). Then for any subensemble of paramagnetic molecules oriented with angles β and γ in the sample reference frame, $\mathbf{g}_{part}^2$-tensor is characterized by

$$\mathbf{g}_{part}(\beta, \gamma)^2 = \mathbf{REu}(0, \beta, \gamma)^T \mathbf{g}^2 \mathbf{REu}(0, \beta, \gamma) \quad (5)$$

where $\mathbf{REu}(0, \beta, \gamma)$ is the Euler rotation matrix.

The $\mathbf{g}^2$-tensor averaged in accordance with orientation distribution is the following:

$$\mathbf{g}_{av}^{\ 2} = \frac{1}{4\pi} \int_{\beta,\gamma} \mathbf{g}_{part}^{\ 2}(\beta, \gamma) \rho_s(\beta, \gamma) \sin\beta \, d\beta \, d\gamma \quad (6)$$

where orientation distribution $\rho_s(\beta, \gamma)$ is given by expression (2).

Then the observed g-value averaged in accordance with orientation distribution can be calculated as follows:

$$\mathbf{g}_{obs}(\chi) = [\mathbf{H}(\chi) \mathbf{g}_{av}^{\ 2} \mathbf{H}(\chi)]^{1/2} \quad (7)$$

where $\mathbf{H}(\chi)$ is the vector of the magnetic field in the sample reference frame and $\mathbf{H}_x(\chi) = \{0, \sin\chi, \cos\chi\}$ and $\mathbf{H}_z(\chi) = \{\cos\chi, \sin\chi, 0\}$ are for X-dependence and Z-dependence, respectively.

For calculations of $\mathbf{g}_{obs}(\chi)$, the values of orientation order parameters S_{20} and S_{22} (eq 2) should be estimated. It is known that the biaxial term S_{22} is often negligible. The value S_{20} for smectic phases is ordinarily within the range of 0.6−0.8 (see for example ref 50). It was found earlier[40] that the value of S_{20} for studied substancies lies in the same range. In the course of fitting experimental dependency values $S_{20} = 0.67$ and $S_{22} = 0$ were obtained. Results of calculations with the use of these values according to eq 7 are presented in Figure 7a as lines.

In the case of the N* phase, the one-particle orientation distribution function should be averaged over the helical orientation structure of the sample. Averaged order parameters for the considered case are the following: $(S_{20})_{av} = S_{20}/4$ and $(S_{22})_{av} = (3/2)^{1/2} S_{20}/4$ (see Appendix B).

Angular dependences of the g-value for the SmC phase (compound (±)-**2**) and SmC* phase (compound (*S*,*S*)-**2**) are shown in Figure 8. The data obtained from experimental spectra demonstrate a minor contradiction. The position of the samples at turn angle 90° for X-dependence and turn angle 90° for Z-dependence are in fact identical, but the obtained g-values are different. This observation indicates that two samples used for recording of X- and Z- dependences were not identical. Possibly they differed slightly by orientation order, temperature, or prehistory in the course of preparation. To improve this small discrepancy, we have shifted Z-dependences up 0.00025, which is almost within the range of experimental errors.

Figure 8 demonstrates that orientation distribution (2) describes the angular dependences of g-values well. Values of one-particle orientation order parameters obtained in the course of simulation of these dependences are presented in Table 2.

dx.doi.org/10.1021/jp410891s | J. Phys. Chem. B 2014, 118, 1932−1942

Table 2. Order Parameters of Studied Phases in the Reference Frame Presented in Figures 4 and 5

LC phase (compound)	S_{20}	S_{22}
N (compound (±)-**1**)	0.67	0
N* (compound (*S*,*S*)- **1**)	0.67 (local)	0 (local)
	0.168 (averaged)	0.205 (averaged)
SmC (compound (±)-**2**)	0.80	−0.07
SmC* (compound (*S*,*S*)-**2**)	0.42	−0.06

It is seen (Figure 7b) that in accordance with the symmetry of the N* sample, the X-dependence of the g-value coincides with Z-dependence. Both nematic phases demonstrate axial local orientation order. Both SmC phases display biaxiality that manifests itself in a nonzero value of order parameter S_{22} that describes the Z-dependence of the observed g-value. It can be seen in Figure 8 that angular dependences in the case of compound (*S*,*S*)-**2** qualitatively resemble the dependences for compound (±)-**2** but are characterized by lower ordering.

Thus, description of angular dependence of g-values gives the quantitative characteristics of molecular orientation distribution. However, the one-particle orientation distribution function ρ_s carries very limited information concerning the molecular structure of the LC phase.

7. DESCRIPTION OF LINE WIDTH ANGULAR DEPENDENCES

Angular dependences of width of EPR spectra are presented in Figure 9.

For description of these angular dependences, we have used direct numerical calculation of EPR spectrum shape. Let an individual EPR line from a solitary magnetic center be a Gaussian line with width δ_G. The line shape in this case is described by the following expressions:

$$\text{Gaus} = \frac{x}{{\delta_G}^3}\exp\left[-\frac{x^2}{2{\delta_G}^2}\right] \rightarrow \text{GausF} = iw\exp\left[-\frac{1}{2}{\delta_G}^2 w^2\right] \quad (8)$$

where x is the magnetic field relative to the center of the line and GausF is the Fourier transform.

The Gaussian shape here has been chosen only for simplification of calculation procedure. Indeed, a δ-function or Lorentzian function could be taken as well. Width of this individual line will be taken below as negligibly small relative to the width of the observed broadened line. Thus, the shape of the initial individual line does not influence the final spectrum.

As is mentioned above, line width of the considered EPR spectra is defined by rotation collisions and by spin exchange and dipole−dipole interactions between LC molecules. The frequency of the rotational collisions is orientation-independent. The rotational collisions define the lifetime of spin states and induce the constant width δ_L of line with Lorentzian shape in accordance with the following expression:

$$\text{Lor} = \frac{\sqrt{2/\pi}}{\delta_L}\frac{1}{1+(x/\delta_L)^2} \rightarrow \text{LorF} = \exp[-\delta_L|w|] \quad (9)$$

The angular dependence is observed as a result of dipole−dipole interaction of molecules that are partners in spin exchange. Such neighboring spin induces an additional magnetic field in the point of considered paramagnetic center. This additional field is known to be described by the following expression:

$$H_{dd} = \mu\frac{3\cos(Hr)^2 - 1}{|r(\psi, \varphi, a_m, \sigma, \alpha_L)|^3} \quad (10)$$

where (Hr) is the angle between the external magnetic field and vector **r** which connects two neighboring centers.

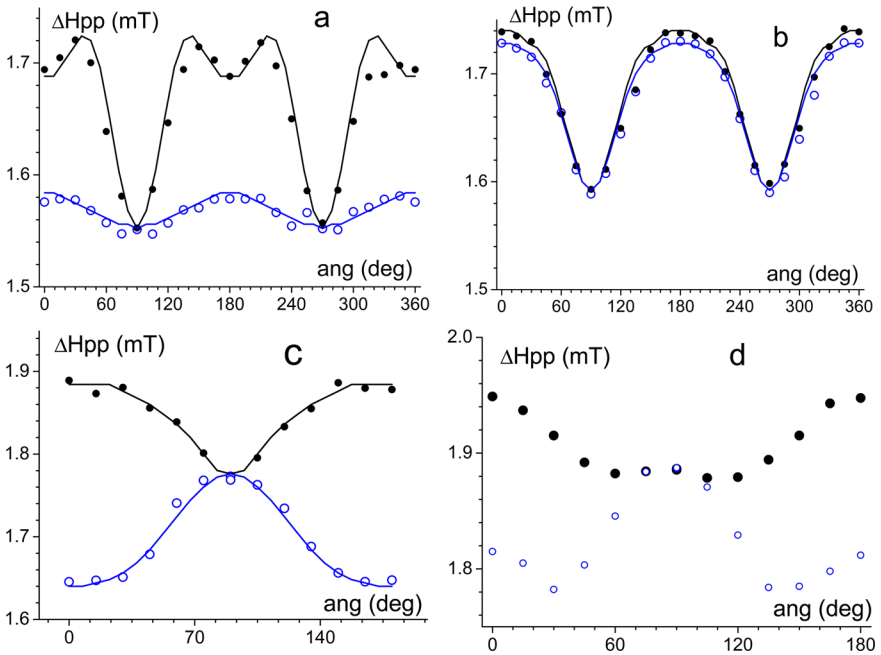

Figure 9. Angular dependences of width of EPR spectra for N (a), N* (b), SmC (c), and SmC* (d) phases. Points are values obtained from experimental spectra; solid points represent rotation around the Xs axis (X-dependence) and open points represent rotation around the Zs axis (Z-dependence). Lines are results of calculations.

dx.doi.org/10.1021/jp410891s | J. Phys. Chem. B 2014, 118, 1932−1942

Table 3. Structural Parameters of Mesophases Obtained in the Course of Description of Experimental Line Width Angular Dependences

LC phase (compound)	δ_L (mT)	a_m (Å)	b_m (Å)	r_m (Å)	σ	α_L	P_{22}
N (compound (±)-**1**)	1.28	7.0	10.0	12.2	55°	0	0.35
N* (compound (*S*,*S*)- **1**)	1.26	6.4	9.1	11.2	55°	0	0.0
SmC (compound (±)-**2**)	1.30	6.5	11.3	13.0	60°	33°	−0.2

Length of vector **r** is in the denominator of eq 10. Here we stress the dependence of the vector **r** on structural parameters described above. Cosine in the numerator of eq 10 is calculated as the dot product of direction cosines of vector **r** (eq 4) and magnetic field vector $\mathbf{H}_x(\chi) = \{0, \sin\chi, \cos\chi\}$, $\mathbf{H}_y(\chi) = \{\sin\chi, 0, \cos\chi\}$, and $\mathbf{H}_z(\chi) = \{\sin\chi, 0, \cos\chi\}$ for angular dependences around Xs, Ys, and Zs axes, respectively.

As two possible spin states are possible for the neighboring center, the presence of a neighbor induces splitting of the EPR line into two components. For example, if the initial line was δ-function, the dipole−dipole interaction with one center results in the following doublet spectrum:

$$H_{dd} = \frac{1}{2}\left[\delta\left(x - \frac{H_{dd}}{2}\right) + \delta\left(x + \frac{H_{dd}}{2}\right)\right] \rightarrow \mathrm{H_{dd}F} = \cos\left(w\frac{H_{dd}}{2}\right) \quad (11)$$

where H_{dd} is given by eq 10 and $\mathrm{H_{dd}F}$ is its Fourier transform.

The resulting spectrum is a convolution of functions 8, 9, and 11. Fourier transform for the resulting spectrum SF is presented as follows:[44]

$$\mathrm{SF}(\chi) = \sum_{\text{layers}} \frac{1}{\pi}\int_{\varphi=0}^{\pi} \mathrm{GausF}\cdot\mathrm{LorF}\cdot\mathrm{H_{dd}F}(\varphi,\chi)\cdot\rho_p(\varphi)\cdot d\varphi \quad (12)$$

where integration over φ reflects the summation of spectra with different orientations of pairs and angle χ describes the angular dependence of the spectrum.

Equation 12 contains the distribution function $\rho_p(\varphi)$. It should be noted that this function is not the one-particle orientation distribution function which was discussed in sections 5 and 6 of present paper. The orientation distribution of vector **r**, which connects neighboring paramagnetic centers, should be used in eq 12. Thus, it is a two-particle distribution function. In our calculations, we used not the full two-particle distribution function but only the partial dependence $\rho_p(\varphi)$ which describes the distribution of projections of vector **r** on plane XsYs. This function was taken as follows:

$$\rho_p(\varphi) = 1 + P_{22}\cos 2\varphi \quad (13)$$

where P_{22} is the two-particle order parameter.

To take into account dipole−dipole interaction from two or more neighboring molecules, the term $\mathrm{H_{dd}F}$ in eq 12 was used two or more times. Each layer with specific orientation was described as a separate integrand in eq 12, and results were summed over all possible layers (Figure 5). The spectrum shape was obtained by numerical inverse Fourier transform of the result of eq 12.

The spectra calculated using this procedure with properly chosen values of parameters were found to be in very good agreement with the spectra obtained in the experiment. Lorentzian and Gaussian widths of calculated spectra in comparison with the same values for experimental spectra are presented in Table 1. Peak-to-peak width of calculated spectra for the purpose of comparison with experimental data was straightforwardly measured as difference of fields for maximum and minimum points of the spectral curve. Angular dependences of the ΔH_{pp} value for calculated spectra are presented in Figure 9 as lines. Dependence of line width in the course of rotation around Ys axis (Y-dependence), which was not studied experimentally, can be calculated, too (see Appendix D).

It was found that the experimental data in the case of the nematic phase (Figure 9a) are described satisfactorily if only one neighboring molecule inducing dipole−dipole interaction is taken into account. This means that in the nematic phase the average number of molecules coupled by spin exchange is equal to two.

In the case of the N* phase (Figure 9b), helical structure induces the new symmetry axis that is parallel to the sample axis Ys. The EPR spectrum in this case is the sum of the spectra with different angles of turn around the Ys axis. Therefore, to calculate spectra, vector **r** (eq 3) should be transformed by rotation around Ys with angle α_Y and used for determination of H_{dd} (eqs 10 and 11). The obtained expression is substituted in eq 12, which then is integrated additionally over variable α_Y. The small difference between X- and Z-dependences in Figure 9b is obviously caused by the presence of two command surfaces. The two command surfaces lead to somewhat larger number of molecules oriented vertically relative to the number of molecules oriented horizontally. This circumstance was taken into account in the following way. In the course of integration over α_Y with the use of the trapezoid method (21 grid points), the spectra at $\alpha_Y = 0$ and $\alpha_Y = \pi$ were taken with coefficient 1 instead of coefficient 0.5. In this way we slightly increased the weight of the spectra from vertically aligned material in the course of integration.

The experimental data for SmC phase (Figure 9c) were found to be satisfactorily described when dipole−dipole interactions with two neighboring molecules were included. These two influencing neighbors are located in opposite directions, as is presented in Figure 6. It was found as well that correct experimental Z-dependence is reproduced only if the smectic layer has limit case 1 orientation (angle $\psi = 0$, see Figure 5a).

The dependence for SmC* phase (Figure 9d) was not described yet as we do not have information concerning the type of structural organization in this medium. As was mentioned above, structural requirements and boundary conditions cannot be satisfied simultaneously in the case of SmC* phase. The resulting structural distortions manifest themselves as diminished orientation order demonstrated in section 6 and as specific features of angular dependence that are seen in Figure 9d. Knowledge of the nature of these distortions is necessary for quantitative description of the observed spectra.

Values of structural parameters were chosen in the course of description of experimental angular dependences. The values corresponding to the best descriptions are collected in Table 3.

dx.doi.org/10.1021/jp410891s | J. Phys. Chem. B 2014, 118, 1932−1942

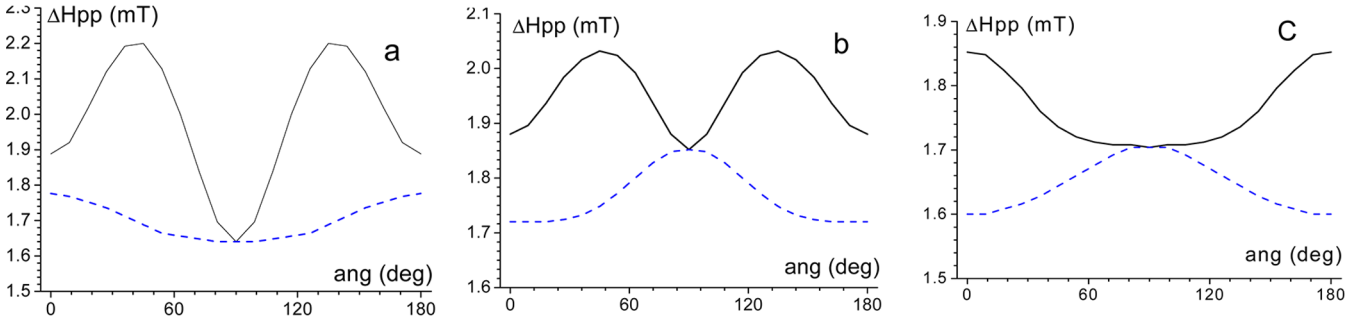

Figure 10. Change of angular dependence when parameter value is changed. $\psi = \pi/2$, $\sigma = 60°$ (limit case 2) (a); $\psi = 0$, $\sigma = 58°$ (limit case 1) (b); $\psi = 0$, $\sigma = 62°$ (limit case 1) (c); other parameters are optimal for SmC phase (Figure 9c, Table 3). X-dependences are solid lines, Z-dependences are dash lines.

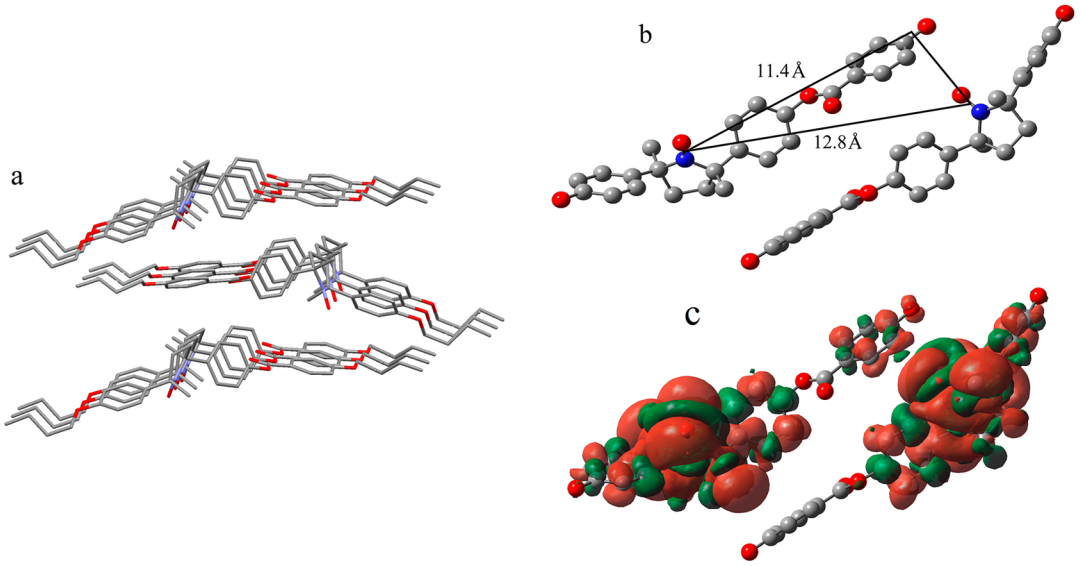

Figure 11. Crystal structure of (*S*,*S*)-**3** determined by X-ray crystallographic analysis (a), relative position of a pair of molecules in the crystal (b), and spin density distribution in the same pair by quantum chemical calculations (c). The hydrocarbon chains are omitted for clarity in panels b and c.

The used method was found to be very sensitive to parameter values. Figure 10 demonstrates the changes of angular dependences brought about by the change of parameters. The dependences presented in Figure 10 should be compared with dependences shown in Figure 9c. Essential changes in the shape of angular dependences induced by variation of parameters are seen. The influence of other parameters is illustrated in Appendix E.

8. INTERMOLECULAR INTERACTIONS IN LC PHASES

On the basis of the structural parameters of mesophases listed in Table 3, the relative molecular alignment in the liquid crystal phases can be estimated. For comparison and reference, the molecular structure and crystal packing of an analogous compound (*S*,*S*)-**3** determined by X-ray crystallographic analysis are used (Figure 11a).[30] We have picked out a pair of molecules in the crystal lattice, which can satisfy the parameters in Table 3. The chosen pair consists of two molecules in the adjacent layers shown in Figure 11a. The distance (12.8 Å) between the paramagnetic nitroxide moieties of the two molecules is in good agreement with the values (r_m) in Table 3 obtained from the EPR spectra. It is easily envisaged that the LC phases are formed by a sequence of such pairs of molecules which continuously change the partners during molecular rotation.

A negative value of order parameter P_{22} for the SmC phase indicates that vector **r** connecting interacting molecules lies predominantly in the plane of the command surfaces. Taking into account that the limit case 1 (Figure 5a) is realized in our experiments, it is clear that vector **r** tends to be in one plane with the director and C-director of the SmC phase. In contrast, the N phase is characterized by a positive P_{22} value. This means that the projection of vector **r** on plane XsYs in the N phase tends to orient perpendicular to command surfaces. Thus, two-particle distribution demonstrates small biaxiality of the SmC and N phases.

It was found that in the case of the SmC phase any paramagnetic center is in spin exchange with two neighboring molecules. Therefore, long chains of molecules undergoing the spin exchange are formed in the SmC layer. As the obtained structural parameters for the N and N* phase are close to those of the SmC phase, one can conclude that similar intermolecular interactions operate in these phases, too. However, a molecule in the N and N* phases on average undergoes the spin exchange with only one neighboring molecule.

An important question is how the molecules in such pairs demonstrate spin exchange in spite of large distance between paramagnetic centers. To clarify this issue we performed quantum chemical calculations of spin density distribution in the studied molecule. DFT calculations were done using the ORCA program package[51] using the B3LYP functional with 6-31G basis modified to describe nitroxide radicals.[52] Calculations were performed for molecular geometry obtained by

dx.doi.org/10.1021/jp410891s | J. Phys. Chem. B 2014, 118, 1932−1942

X-ray data (published in Supporting Information of ref 30.). The results of calculation for a single molecule have shown that the spin density is completely localized near the nitroxide group. However, calculation for the molecular pair presented in Figure 11c proves that appreciable spin density is transferred on the distant aromatic ring in one molecule of the pair. This spin polarization mechanism is most likely responsible for the generation of positive magneto-LC effects.[30−32]

9. CONCLUSIONS

To gain an insight into the origin of positive magneto-LC effects operating in the LC phases of paramagnetic organic materials, the structural parameters of the LC phases have been determined by quantitative analysis of angular dependences of g-value and line width of EPR spectra of compounds **1** and **2** and by DFT calculations of spin density distribution in the interacting molecules based on the crystal structure. Consequently, it has been concluded that an intermolecular spin polarization mechanism operating between the central paramagnetic center of one molecule and the aromatic ring of another molecule, rather than the direct through-space interactions between the paramagnetic centers, contributes to the occurrence of the positive magneto-LC effects.

In addition, EPR spectroscopy has proved to be an excellent tool for analyzing the microscopic dynamic behavior of molecules and magnetic interactions in the LC materials because the spin exchange and dipole−dipole interactions of paramagnetic centers manifest themselves in the shape of the EPR spectrum. In the near future, the EPR techniques employed here will be applied to the characterization of novel metal-free soft materials, such as ionic LCs, micelles, emulsions, and gels, which will be developed on the basis of the nitroxide radical chemistry.

APPENDIX A

Calculation of Magnetic Parameters Averaged by Rotation

g-Tensor and tensor of hfi are averaged by rotation around the long molecular axis. In the magnetic frame

$$\mathbf{g}^2 = \begin{pmatrix} g_{xx}^2 & 0 & 0 \\ 0 & g_{yy}^2 & 0 \\ 0 & 0 & g_{zz}^2 \end{pmatrix}, \quad \mathbf{A} = \begin{pmatrix} A_{xx} & 0 & 0 \\ 0 & A_{yy} & 0 \\ 0 & 0 & A_{zz} \end{pmatrix} \tag{A1}$$

where $g_{xx} = 2.0093$, $g_{yy} = 2.0063$, $g_{zz} = 2.0023$, $A_{xx} = 0.5$ mT, $A_{yy} = 0.5$ mT, and $A_{zz} = 3.22$ mT.

If the Euler rotation matrix is designated as $\mathbf{REu}(\alpha, \beta, \gamma)$, tensors in the rotation frame are

$$\begin{aligned} \mathbf{g_{rf}}^2 &= \mathbf{REu}(\alpha, \beta, \gamma)^{\mathrm{T}} \mathbf{g}^2 \mathbf{REu}(\alpha, \beta, \gamma) \\ \mathbf{A_{rf}} &= \mathbf{REu}(\alpha, \beta, \gamma)^{\mathrm{T}} \mathbf{A} \mathbf{REu}(\alpha, \beta, \gamma) \end{aligned} \tag{A.2}$$

where index T means transposed matrix.

Let the matrix for rotation around the z axis be

$$\mathbf{R}_z = \begin{pmatrix} \cos\varphi & \sin\varphi & 0 \\ -\sin\varphi & \cos\varphi & 0 \\ 0 & 0 & 1 \end{pmatrix}$$

Then tensors averaged in the course of uniform rotation around z axis are

$$\begin{aligned} \mathbf{g}_{\mathbf{R}}^2 &= \int_{\varphi} \mathbf{R}_z(\varphi)^{\mathrm{T}} \mathbf{g_{rf}}^2 \mathbf{R}_z(\varphi)\, \mathrm{d}\varphi \\ \mathbf{A}_{\mathbf{R}} &= \int_{\varphi} \mathbf{R}_z(\varphi)^{\mathrm{T}} \mathbf{A_{rf}} \mathbf{R}_z(\varphi)\, \mathrm{d}\varphi \end{aligned} \tag{A3}$$

Taking into account that the experimentally determined tilt angles for rotation axis are $\alpha = 90°$ and $\beta = 39.6°$, magnetic tensors averaged by rotation are $g_{xx} = 2.0068$, $g_{yy} = 2.0068$, $g_{zz} = 2.0037$, $A_{xx} = 0.94$ mT, $A_{yy} = 0.94$ mT, and $A_{zz} = 2.03$ mT.

APPENDIX B

Calculation of Order Parameter Averaged over Helical Structure of Nematic Phase

In accordance with summation theorem of Wigner's D-matrix, under the turn of the reference frame by angle θ around the Ys axis, the orientation distribution function is characterized by the following new order parameters:

$$s'^{j}_{mn}(\theta) = \sum_{k=-j}^{j} s^{j}_{kn} d^{j}_{k,m}(\theta) \tag{B1}$$

where s^j_{kn} are order parameters for initial distribution function presented as a series of Wigner's D-matrix, $s'^j_{kn}(\theta)$ order parameters for reference frame turned by angle θ, and $d^j_{k,m}(\theta)$ elements of Wigner's D-matrix.

The integration over angle θ is averaging of orientation distribution function over helical structure N* phase:

$$(s^{j}_{mn})_{\mathrm{av}} = \frac{1}{\pi} \int_{\theta} s'^{j}_{mn}(\theta)\, \mathrm{d}\theta \tag{B2}$$

Let s^j_{kn} be the local order parameters characterizing the nematic phase, then $(s^j_{mn})_{\mathrm{av}}$ are order parameters for the N* phase in the sample reference frame presented in Figure 4b.

Taking into account that the local nematic distribution is assumed to be axial and only rank two terms are used, it is seen that the sum in eq B1 and consequently in eq B2 contains only one summand. Additionally, when the molecule is considered as axial, the third index can be omitted. In accordance with B2, the rank two order parameter is as follows:

$$(S_{2\mathrm{m}})_{\mathrm{av}} \equiv (s^2_{0\mathrm{n}})_{\mathrm{av}} = \frac{S_{20}}{\pi} \int_{\theta} d^2_{0n}(\theta)\, \mathrm{d}\theta \tag{B3}$$

APPENDIX C

Calculation of Vector r in the Case of SmC Phase

Dependence of length of **r** vector can be obtained using the simple geometrical consideration presented in Figure C1.

Figure C1 represents two nitroxide groups (marked as large points) incorporated in the structure of the SmC layer. The plane of the layer is marked as PL. This plane is tilted by α_L relative to plane XsYs of the sample (see Figure 5). Angle φ describes the

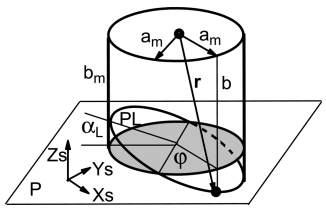

Figure C1. Determination of vector which connects two nitroxide moieties in the neighboring molecules.

dx.doi.org/10.1021/jp410891s | J. Phys. Chem. B 2014, 118, 1932−1942

direction to the neighboring molecule in the layer. Angle φ for different pairs of neighboring molecules takes an arbitrary value. The components of vector **r** are $\mathbf{a}_m$ and **b**. From geometrical consideration, value **b** is calculated as:

$$\mathbf{b} = \mathbf{b}_m + \mathbf{a}_m \sin\varphi tg\alpha_m \quad \text{(C1)}$$

Taking into account that angle ψ (not shown in Figure C1) describes the orientation of the layer in the sample reference frame (Xs, Ys, Zs), one can obtain eq 3.

APPENDIX D

Angular Dependence of Line Width for Rotation about the *y* Axis

The calculated Y-dependence, which was not studied experimentally, in the case of the SmC phase is presented in Figure D1.

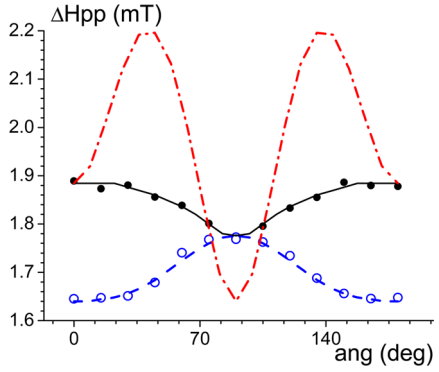

Figure D1. Calculated dependences of line width on rotation angle around different axes: *x* axis (solid line), *y* axis (dash dot line), and *z* axis (dash line).

APPENDIX E

Influence of Parameter Values on Calculated Angular Dependencies

Angular dependences of the width of EPR spectra calculated with different values of a_m and α_L are shown in Figures E1 and E2, respectively.

AUTHOR INFORMATION

Corresponding Author

*Phone: +7(495)9394900. E-mail: a.kh.vorobiev@gmail.com.

Notes

The authors declare no competing financial interest.

ACKNOWLEDGMENTS

The financial support of RFBR (Grants a-14-03-00323, mol-a-12-03-31114, mol-a-14-02-31882) is gratefully acknowledged. Some numerical calculations were performed with the use of Lomonosov Supercomputer at Moscow University. We thank Dr. Oleg Gromov for helpful discussion.

REFERENCES

(1) Tschierske, C. Theme Issue: Liquid Crystals Beyond Display Applications. *J. Mater. Chem.* **2008**, *18*, 2869−2971.
(2) Feringa, B. L.; Jager, W. F.; de Lange, B. Organic Materials for Reversible Optical Data Storage. *Tetrahedron* **1993**, *49*, 8267−8310.
(3) *Liquid Crystals: Frontiers in Biomedical Applications*; Woltman, S. J., Jay, G. D., Crawford, G. P., Eds.; World Scientific: Singapore, 2007.
(4) Kippelen, B.; Yoo, S.; Haddock, J. A.; Domercq, B.; Barlow, S.; Minch, B.; Xia, W.; Marder. S. R.; Armstrong, N. R. In *Organic Photovoltaics: Mechanism, Materials and Devices*; Sun, S.-S., Sacriciftci, N. S., Eds.; CRC Press: Boca Raton, FL, 2005; p 271.

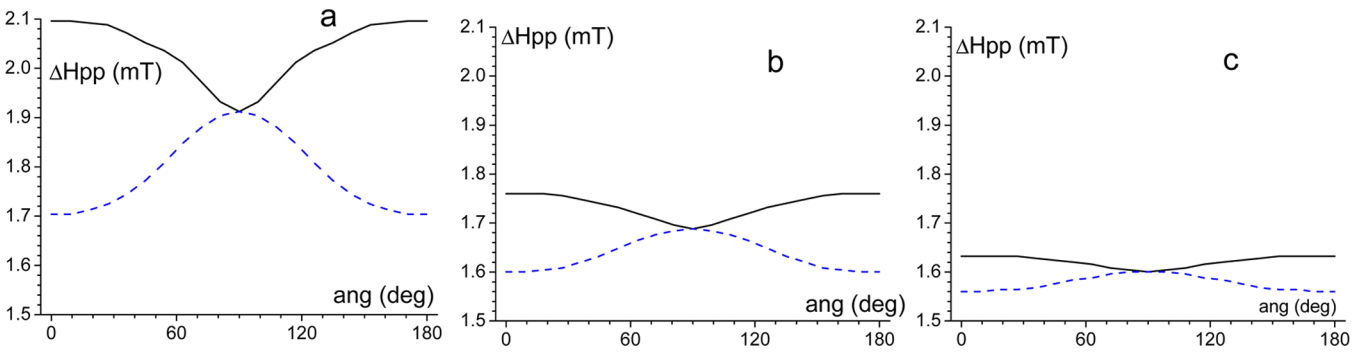

Figure E1. Angular dependences of width of EPR spectra calculated with different values of a_m: a_m = 6 Å (a), a_m = 7 Å (b), a_m = 8 Å (c). Other parameters are optimal for the SmC phase (Table 3). X-dependences are solid lines, and Z-dependences are dashed lines.

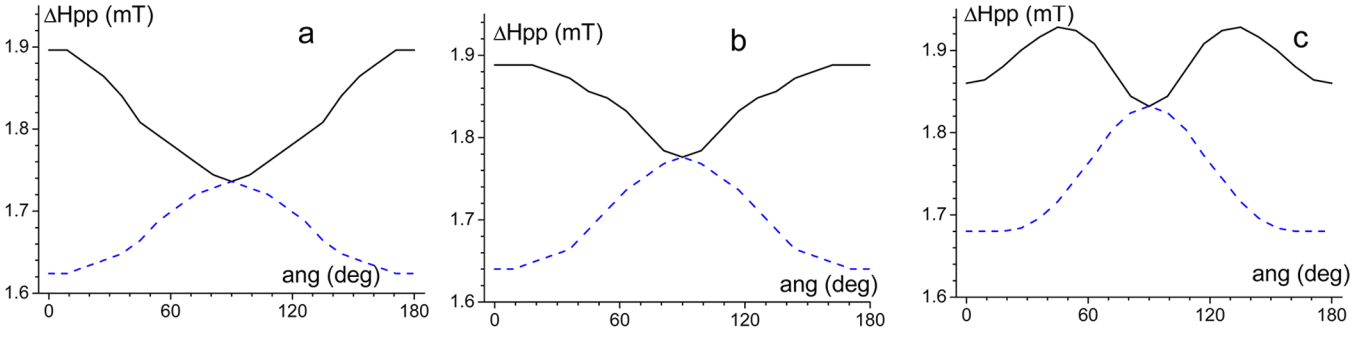

Figure E2. Angular dependences of width of EPR spectra calculated with different values of α_L: α_L = 29° (a), α_L = 33° (b), α_L = 37° (c). Other parameters are optimal for the SmC phase (Table 3). X-dependences are solid lines, and Z-dependences are dashed lines.

dx.doi.org/10.1021/jp410891s | *J. Phys. Chem. B* 2014, 118, 1932−1942

(5) Blinov, L. M. *Electro-Optical and Magneto-Optical Properties of Liquid Crystals*; John Wiley & Sons: New York, 1983.
(6) Chandrasekhar, S. *Liquid Crystals*, 2nd ed.; Cambridge University Press: Cambridge, 1992.
(7) *Physical Properties of Liquid Crystals*; Demus, D., Goodby, J., Gray, G. W., Spiess, H.-W., Vill, V., Eds.; Wiley-VCH: Weinheim, Germany, 1999.
(8) Dierking, I. *Textures of Liquid Crystals*; Wiley-VCH: Weinheim, Germany, 2003.
(9) Eerenstein, W.; Mathur, N. D.; Scott, J. F. Multiferroic and Magnetoelectric Materials. *Nature* **2006**, *442*, 759−765.
(10) Rao, C. N. R.; Serrao, C. R. New Routes to Multiferroics. *J. Mater. Chem.* **2007**, *17*, 4931−4938.
(11) Felser, C.; Fecher, G. H.; Balke, B. Sprintronics: A Challenge for Material Science and Solid-State Chemistry. *Angew. Chem., Int. Ed.* **2007**, *46*, 668−699.
(12) Rikken, G. L. J. A.; Raupach, E. Observation of Magneto-Chiral Dichroism. *Nature* **1997**, *390*, 493−494.
(13) Rikken, G. L. J. A.; Raupach, E. Enantioselective Magnetochiral Photochemistry. *Nature* **2000**, *405*, 932−935.
(14) Train, C.; Gheorghe, R.; Krstic, V.; Chamoreau, L.-M.; Ovanesyan, N. S.; Rikken, G. L. J. A.; Gruselle, M.; Verdaguer, M. Strong Magneto-Chiral Dichroism in Enantiopure Chiral Ferromagnets. *Nat. Mater.* **2008**, *7*, 729−734.
(15) Deutsch, M. Orientational Order Determination in Liquid Crystals by X-Ray Diffraction. *Phys. Rev. A.* **1999**, *44*, 8264−8270.
(16) Hamley, I. W.; Garnett, S.; Luckhurst, G. R.; Roskilly, S. J.; Pedersen, J. S.; Richardson, R. M.; Seddon, J. M. Orientational Ordering in the Nematic Phase of a Thermotropic Liquid Crystal: A Small Angle Neutron Scattering Study. *J. Chem. Phys.* **1996**, *104*, 10046−10054.
(17) Michl, J.; Thulstrup, E. W. *Spectroscopy With Polarized Light: Solute Alignment by Photoselection in Liquid Crystals, Polymers and Membranes*; VCH Publishers: New York, 1986.
(18) Southern, C. D.; Gleeson, H. F. Using the Full Raman Depolarization of the Order Parameters in Liquid Crystal Systems. *Eur. Phys. J. E* **2007**, *24*, 119−128.
(19) Wertz, J. E.; Bolton, J. R. *Electron Spin Resonance: Elementary Theory and Practical Applications*; Chapman and Hall: New York, 1986.
(20) Molin, Y. N.; Salikhov, K. M.; Zamaraev, K. I. *Spin Exchange: Principles and Applications in Chemistry and Biology*; Springer-Verlag: New York, 1980; Vol. *8*.
(21) Nayeem, Akbar; Rananavare, S. B.; Sastry, V. S. S.; Freed, Jack H. Heisenberg Spin Exchange and Molecular Diffusion in Liquid Crystals. *J. Chem. Phys.* **1989**, *91* (11), 6887−6905.
(22) Anderson, P. W. A Mathematical Model for the Narrowing of Spectral Lines by Exchange or Motion. *J. Phys. Soc. Jpn.* **1954**, *9*, 316−339.
(23) Kivelson, D. Theory of ESR Linewidths of Free Radicals. *J. Chem. Phys.* **1960**, *33*, 1094−1106.
(24) Stößer, R.; Herrmann, W.; Pahlke, A. Spin Exchange of Nitroxyl Radicals in H_2O and D_2O. *J. Phys. Chem. A.* **2012**, *116*, 952−961.
(25) Bales, B. L.; Peric, M. EPR Line Shifts and Line Shape Changes due to Spin Exchange of Nitroxide Free Radicals in Liquids. *J. Phys. Chem. B.* **1997**, *101*, 8707−8716.
(26) Grant, W. J. C.; Strandberg, M. W. P. Statistical Theory of Spin-Spin Interactions in Solids. *Phys. Rev.* **1964**, *135* (3A), 715−726.
(27) Mao, C. R.; Kreilick, R. W. Exchange and Dipolar Interactions in a Solid Nitroxide Radical. *Chem. Phys. Let.* **1975**, *34* (3), 447−450.
(28) Salikhov, K. M. Contributions of Exchange and Dipole-Dipole Interactions to the Shape of EPR Spectra of Free Radicals in Diluted Solutions. *Appl. Magn. Reson.* **2010**, *38*, 237−256.
(29) Van Vleck, J. H. The Dipolar Broadening of Magnetic Resonance Lines in Crystals. *Phys. Rev.* **1948**, *74* (9), 1168−1183.
(30) Ikuma, N.; Tamura, R.; Shimono, S.; Kawame, N.; Tamada, O.; Sakai, N.; Yamauchi, J.; Yamamoto, Y. Magnetic Properties of All-Organic Liquid Crystals Containing a Chiral Five-Membering Cyclic Nitroxide Unit Within the Rigid Core. *Angew. Chem., Int. Ed.* **2004**, *43*, 3677−3682.
(31) Ikuma, N.; Tamura, R.; Shimono, S.; Uchida, Y.; Masaki, K.; Yamauchi, J.; Aoki, Y.; Nohira, H. Ferroelectric Properties of Paramagnetic, All-Organic, Chiral Nitroxyl Radical Liquid Crystals. *Adv. Matter* **2006**, *18*, 477−480.
(32) Uchida, Y.; Suzuki, K.; Tamura, R.; Ikuma, N.; Shimono, S.; Noda, Y.; Yamauchi, J. Anisotropic and Inhomogeneous Magnetic Interactions Observed in All-Organic Nitroxide Radical Liquid Crystals. *J. Am. Chem. Soc.* **2010**, *132*, 9746−9752.
(33) Tamura, R.; Suzuki, K.; Uchida, Y. In *Handbook of Liquid Crystals*, 2nd ed.; Goodby, J., Kato, T., et al., Eds.; Wiley-VCH: Weinheim, Germnay, 2014.
(34) Tamura, R.; Suzuki, K.; Uchida, Y.; Noda, Y. EPR Characterization of Diamagnetic and Magnetic Organic Soft Materials Using Nitroxide Spin Probe Techniques. *Electron Paramagn. Reson.* **2013**, *23*, 1−21.
(35) Tamura, R.; Uchida, Y.; Suzuki, K. In *Liquid Crystals Beyond Displays: Chemistry, Physics, and Applications*; Li, Q., Ed.; John Wiley & Sons: Hoboken, NJ, 2012; pp 83−110.
(36) Tamura, R.; Uchida, Y.; Suzuki, K. In *Nitroxides - Theory, Experiment and Applications*; Kokorin, A. I., Ed.; INTECH: Rijeka, Croatia, 2012; pp 191−210.
(37) Tamura, R.; Uchida, Y.; Ikuma, N. Paramagnetic All-Organic Chiral Liquid Crystals. *J. Mater. Chem.* **2008**, *18*, 2872−2876.
(38) Chumakova, N. A.; Vorobiev, A. Kh.; Ikuma, N.; Uchida, Y.; Tamura, R. Magnetic Characteristics and Orientation of a New Nitroxide Radical in an Ordered Matrix. *Mendeleev Comm.* **2008**, *18*, 21−23.
(39) Vorobiev, A. Kh.; Yankova, T. S.; Chumakova, N. A. Orientation Distribution Function and Order Parameters of Oriented Spin Probe as Determined by EPR Spectroscopy. *Chem. Phys.* **2012**, *409*, 61−73.
(40) Noda, Y.; Shimono, S.; Baba, M.; Yamauchi, J.; Ikuma, N.; Tamura, R. EPR Studies on Molecular Orientation in a Surface-Stabilized Paramagnetic Liquid Crystal Cell. *J. Phys. Chem. B* **2006**, *110*, 23683−23687.
(41) Noda, Y.; Shimono, S.; Baba, M.; Yamauchi, Y.; Uchida, Y.; Ikuma, N.; Tamura, R. EPR Investigations on Molecular Orientation of Paramagnetic Liquid Crystals in a Surface-Stabilized Liquid Crystal Cell: Studies on a Smectic C or Chiral Smectic C Phase. *Appl. Magn. Reson.* **2008**, *33*, 251−267.
(42) Vorobiev, A. Kh.; Chumakova, N. A. In *Nitroxides - Theory, Experiment and Applications*, Kokorin, A. I., Ed.; INTECH, Rijeka, Croatia, 2012; pp 58−112.
(43) Dobryakov, S. N.; Lebedev, Ya. S. Analysis of Spectral Lines Whose Profile is Described by a Composition of Gaussian and Lorentz Profiles. *Dokl. Akad. Nauk SSSR* **1968**, *182*, 62.
(44) Jidomirov, G. M.; Lebedev, Ya. S.; Dobryakov, S. N.; Shteinshneider, N. Ya.; Chirkov, A. K.; Gubanov, V. A. *Interpretation of Complex ESR Spectra*; Nauka: Moscow, 1975; p 216 (in Russsian).
(45) Abragam, A.; Bleaney, B. *Electron Paramagnetic Resonance of Transition Ions*; Clarendon Press: Oxford, U.K., 1970.
(46) Schneider, D. J.; Freed, J. H. In *Biological Magnetic Resonance*; Berliner, L. J., Reuben, J., Eds.; Plenum: New York, 1989; Vol. *8*, pp 1−76.
(47) Budil, F. D. E.; Lee, S.; Saxena, S.; Freed, J. H. Nonlinear-Least-Squares Analysis of Slow-Motion EPR Spectra in One and Two Dimensions Using a Modified Levenberg-Marquardt Algorithm. *J. Magn. Reson., Ser. A* **1996**, *120*, 155−189.
(48) Zannoni, C. In *The Molecular Physics of Liquid Crystals*; Luckhurst, G. R., Gray, G. W., Eds.; Academic Press, London, 1979; p 51.
(49) Barois, P.; Pommier, J.; Prost, J. In *Solitons in Liquid Crystals*; Lam, L., Prost, J., Eds.; Springer: New York, 1992; p 190.
(50) Bielejewska, N.; Chrzumnicka, E.; Mykowska, E.; Przybylski, R.; Szybowicz, M.; Wladysiak, K.; Bauman, D. Comparative Study of Orientational Order of Some Liquid Crystals from Various Homologous Series. *Acta Phys. Pol., A* **2006**, *110*, 777−793.
(51) Neese, F. The ORCA Program System. *Wiley Interdiscip. Rev.: Comput. Mol. Sci.* **2012**, *2*, 73−78.
(52) Barone, V.; Cimino, P.; Stendardo, E. Development and Validation of the B3LYP/N07D Computational Model for Structure Parameter and Magnetic Tensors of Large Free Radicals. *J. Chem. Theory Comput.* **2008**, *4*, 751−764.